한국표면공학회지
Journal of the Korean Institute of Surface Engineering
Vol. 31, No. 6, Dec. 1998
<연구논문>

Evolution of surface morphology and roughness in Si and $Si_{0.7}Ge_{0.3}$ thin films

N. E. Lee

School of Metallurgical and Materials Engineering
Sungkyunkwan University, 300 Chunchun-dong, Suwon, Kyunggi 440-746, Korea

Si 및 $Si_{0.7}Ge_{0.3}$ 박막의 표면형태 및 조도의 전개

이 내 응

성균관대학교, 금속·재료공학부

Abstract

The evolution of surface roughness and morphology in epitaxial Si and $Si_{0.7}Ge_{0.3}$ alloys grown by UHV ion-beam sputter deposition onto nominally-singular, [100]-, and [110]-miscut Si(001) was investigated by atomic force microscopy and transmission electron microscopy. The evolution of surface roughness of epitaxial Si films grown at 300℃ is inconsistent with conventional scaling and hyperscaling laws for kinetic roughening. Unstable growth leading to the formation of mounds separated by a well-defined length scale is observed on all substrates. Contrary to previous high-temperature growth results, the presence of steps during deposition at 300℃ increases the tendency toward unstable growth resulting in a much earlier development of mound structures and larger surface roughnesses on vicinal substrates. Strain-induced surface roughening was found to dominate in $Si_{0.7}Ge_{0.3}$ alloys grown on singular Si(001) substrates at $T_s \geq 450$℃ where the coherent islands are preferentially bounded along ⟨100⟩ directions and exhibit {105} facetting. Increasing the film thickness above critical values for strain relaxation leads to island coalescence and surface smoothening. At very low growth temperatures ($T_s \leq 250$℃), film surfaces roughen kinetically, due to limited adatom diffusivity, but at far lower rates than in the higher-temperature strain-induced regime. There is an intermediate growth temperature range, however, over which alloy film surfaces remain extremely smooth even at thicknesses near critical values for strain relaxation.

1. INTRODUCTION

Surface morphology and roughness evolution during thin film deposition are presently of intense interest in thin film research.[1] While film growth temperatures in modern applications are

being driven toward lower values in order to, for example, obtain abrupt interfaces in multilayer devices, low-temperature growth has generally been found to lead to kinetically roughened surfaces.[2,3] Low-temperature epitaxy studies have concentrated primarily on homoepitaxial systems,[2,3] while most investigations of surface roughening during heteroepitaxy have employed relatively high growth temperatures.[4-11]

Low-temperature growth has sparked intensive theoretical investigation of "kinetic roughening" during epitaxial growth. Much of this work has been based on the assumption that roughening can be modeled using scaling theory applied to growth surfaces which exhibit self-affine characteristics. Under this hypothesis, roughness evolves with a temporal and scale invariant structure.[1] While many experiments on surface roughening during film growth have been interpreted in the context of the dynamic scaling hypothesis, no consensus has emerged concerning the relationship between roughness and growth exponents appropriate to a given growth process.

Thin film growth modes on dissimilar substrates have been characterized based upon equilibrium thermodynamics as two-dimensional (2D), 3-dimensional (3D), and Stranski-Krastanov (SK). In the latter case, heteroepitaxial film growth initially proceeds in a 2D layer-by-layer mode then, driven by the increasing strain component in the total system free energy, switches to 3D. For $Si_{1-x}Ge_x/Si$ (001), the 2D→3D transition thickness h_{S-K} is dependent upon alloy composition x and, hence, directly related to the amount of biaxial film strain.[5] There are some indications that roughening during SK growth can be kinetically limited by lowering the growth temperature T_s[6,7] although no systematic investigations have been reported. Most of the reported experimental investigations on surface morphological evolution during $Si_{1-x}Ge_x$ epitaxy have been limited to relatively high growth temperatures (400-750 ℃) and compositions where surface morphologies are determined primarily by energetics rather than kinetics.[8-10] The authors are unaware of published literature on surface roughening during strained-layer epitaxy of $Si_{1-x}Ge_x$ alloys at low temperatures ($T_s \leq 400$℃).

In this article, we present the results of an AFM investigation of the evolution of surface morphology and roughness in epitaxial Si and $Si_{0.7}Ge_{0.3}$ films deposited on nominally-singular and miscut Si(001). The ion-beam sputter deposition technique proved to be very useful since it yields critical epitaxial Si(001) thicknesses t_e which are an order of magnitude larger than those obtainable by MBE,[12,14] thus allowing roughness measurements to be carried out over a much wider range of layer thicknesses.

2. EXPERIMENTAL PROCEDURE

All film growth experiments were conducted in an UHV three-chamber load-locked stainless-steel system shown schematically elsewhere.[12,13] The growth chamber is cryo-pumped with a base pressure of 1×10^{-10} Torr and contains facilities for reflection high-energy electron diffraction (RHEED) and residual gas analysis. The analytical chamber, which is ion-pumped, is equipped with an Auger electron spectrometer (AES). Sputtering is carried out using

UHV double-grid multi-aperture broad ion-beam sources with provisions for in-situ spatial adjustment.

1 keV Kr^+ ion beams were used to sputter undoped float-zone Si and Ge targets to generate hyperthermal Si and Ge beams. With primary ion beams incident upon their respective targets at a polar angle of 60° and the substrates centered with respect to the erosion craters such that the target and substrate normals formed included angles of 48°, the results of TRIM Monte Carlo simulations showed that the average energy of Si(Ge) atoms incident at the substrate surface is ≃18 (15) eV while backreflected Kr contributes only ≃0.04(0.06) eV per deposited Si(Ge) with $J_{Kr}/J_{Si(Ge)} \simeq 0.003(0.01)$. The composition and growth rate of as-deposited alloy films were controlled by adjusting the current on the each target using precalibrated values obtained by a combination of high-resolution XRD, RBS, and TEM analyses.

The primary substrates used were 15×15×0.5 mm^3 P-doped n-type Si(001) wafers with miscut angle of≃0.14° toward [110] (average terrace length ⟨ℓ⟩=56 nm) and a resistivity of 4-8 Ω-cm. For growth on vicinal substrates, Si(001) wafers with miscuts of 4° toward [100] (⟨ℓ⟩=2 nm) and 4° toward [110] were used. The Si(001)-4°[100] surface consists of terraces bounded by single-atom height steps composed of equal fractions of A and B edges. Substrate cleaning consisted of degreasing followed by a UV ozone treatment. The wafers were then H-passivated by dipping in dilute HF and immediately inserted into the vacuum system. Final substrate preparation included degassing at 200℃ for 1 h followed by hydrogen desorption at 650℃ for 10 s and the growth of 100-nm-thick Si buffer layers. The buffer layer growth temperature was chosen to provide a reproducibly smooth starting surfaces as judged by correlated height-difference measurements (see Fig. 2 below). RHEED patterns were 2×1 with sharp Kikuchi lines. No residual C or O was detected by AES.

Surface morphologies of Si and SiGe alloy films were investigated by atomic force microscopy (AFM). The measurements were carried out using a Digital Nanoscope II microscope operated in air in the contact mode with oxide-sharpened Si_3N_4 tips having radii of 5-40nm. The composition and thickness of each film, accurate to within ±1.2 at% and ±3 at%, respectively, were determined by Rutherford backscattering spectroscopy (RBS). TEM analyses were carried out using a Philips CM-12 operated at 120 kV.

3. RESULTS AND DISCUSSION

3.1 Surface morphology and roughness evolution during Si(001) growth

All Si films used in this investigation were single crystals of high structural quality with no defects observable by conventional or high-resolution TEM and XTEM. Some typical AFM images of the surfaces of Si films grown to different nominal layer thicknesses t on singular and vicinal Si(001) substrates are presented in Fig. 1. The surface morphology of 50-nm-thick layers (not shown) grown on singular substrate is relatively flat with no detectable features. Further growth, however, leads

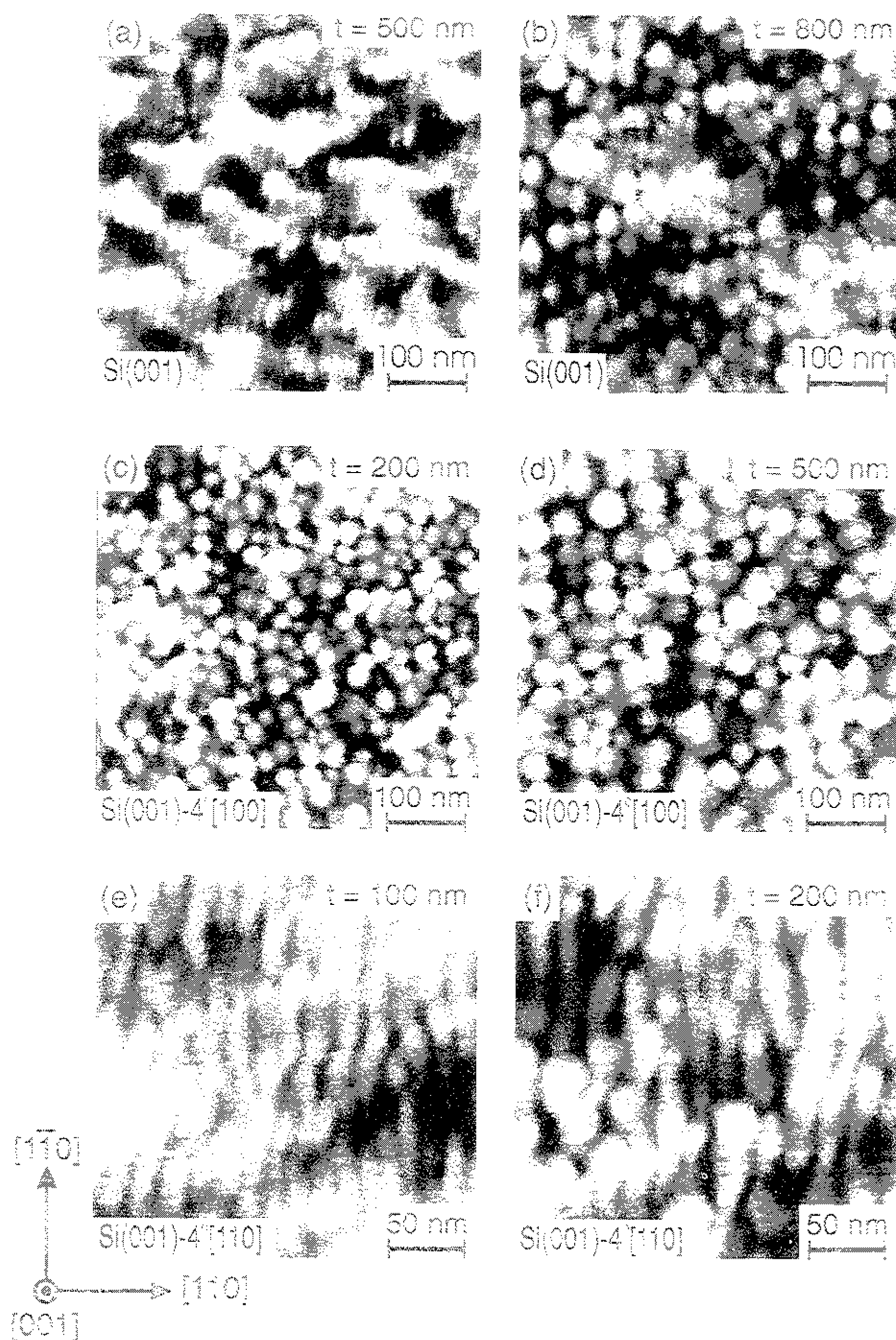

Fig. 1 AFM images of the surfaces of epitaxial Si films grown on Si(001) substrates at T_s=300℃. Substrate miscut direction, film thicknesses, and the black-to-white gray scales are:
(a) singular, 500 nm, 4 nm, (b) singular, 800 nm, 8 nm, (c) [100], 200 nm, 3 nm, (d) [100], 500 nm, 4 nm, (e) [110], 100 nm, 7 nm, and (f) [110], 200 nm, 7 nm.

to the development of features, linearly anisotropic along [110], (see, for example, Fig. 1 (a) corresponding to t=500nm). Compact well-defined growth mounds are clearly observed on singular substrates at t=800nm (Fig. 1 (b)). In contrast, the initiation of mound formation is already evident at t=50nm (not shown) on the [100]-miscut vicinal surface and the mounds continuously coarsen with further deposition as shown in Figs. 1(c) (t=200 nm) and 1(d) (t=500nm). The behavior on the [110]-miscut surface is similar to that of the [100]-miscut except that the mounds exhibit a strong shape anisotropy along the initial [110] step direction as shown in Figs. 1 (e) and 1(f).

In all cases, the growth mounds we observe are compact objects rather than fractal in nature and thus are not expected to obey conventional scaling models for kinetic surface roughening. Nevertheless, the height difference correlation function $G(\rho,t)=\langle|h(j,t)-h(i,t)|^2\rangle$, where ρ is the separation of positions i and j, still provides a quantitative measure of the evolution of surface roughness.[1] The results are presented in Figs. 2(a) and 2(b) as the root-mean correlated height difference $[G(\rho, t)]^{1/2}$ vs ρ in a log-log plot. With the exception of the data for t≤50nm on singular substrates for which no growth mounds were observed, the two sets of curves exhibit similar behavior. $G^{1/2}$ increases with ρ following a power law behavior until saturation is reached for each film thickness. Note that, contrary to the predictions of conventional kinetic roughening models assuming self-affine surfaces,[1] $[G(\rho)]^{1/2}$ increases with increasing t at a given value of

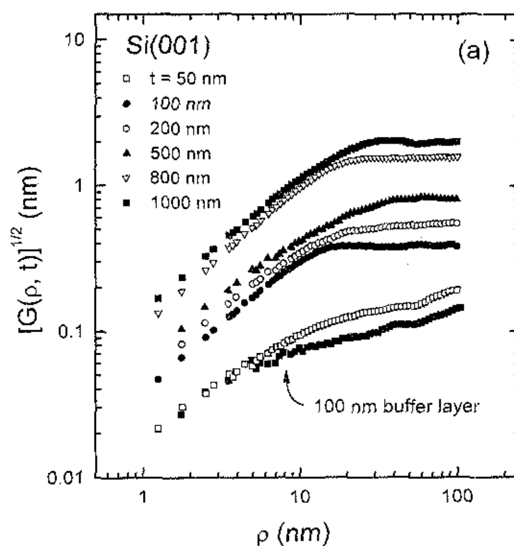

(a)

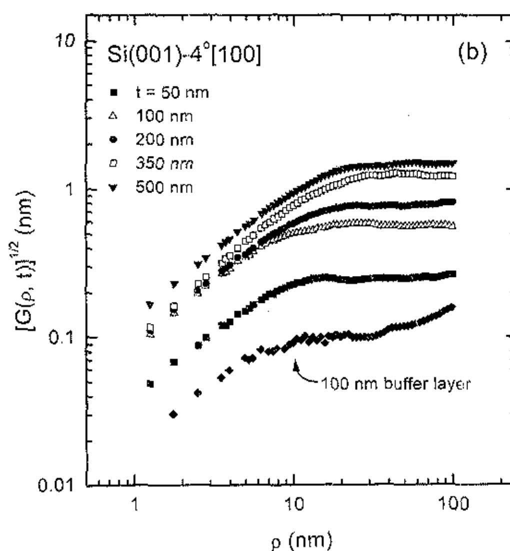

(b)

Fig. 2 Root-mean correlated height-difference $[G(\rho,t)]^{1/2}$ vs the separation ρ of positions i and j on the surfaces of epitaxial Si films grown at 300℃ to thicknesses t=50-1000 nm on (a) nominally-singular and (b) 4° [100]-miscut substrates.

ρ in the presaturation region.

Effective roughening and growth exponents α and β were determined from the data in Fig. 2 and 3 using the scaling relationships $G(\rho,t)\propto\rho^{2\alpha}$ for small ρ and $G(\rho,t)\propto t^{2\beta}$ for $\rho\rightarrow\infty$. $[G(\rho\rightarrow\infty)]^{1/2}$ is defined as the average of all measured $[G(\rho)]^{1/2}$ values obtained for ρ larger than that corresponding to the intersection of best-fit straight lines drawn through the steeply rising and saturation regions of plots. $[G(\rho\rightarrow\infty)]^{1/2}$ is related to the surface width w, $[G(\rho\rightarrow\infty)]^{1/2}\simeq 2^{1/2}w$, where $w=\langle h-\langle h\rangle\rangle^{1/2}$.[16] Physically, α is a measure of how well the roughness can be described by a single lateral length scale (e.g., periodic surface roughness corresponds to α=1). (1,16) $\alpha_{eff}=0.85\pm0.05$ for growth with t=200-1000 nm on singular surfaces and 0.80 ± 0.05 for growth with t=50-500 nm on [100]-miscut surfaces, both remarkably similar to the value obtained for low-temperature MBE Ge growth on Ge(001), 0.80 ± 0.05.[3] $[G(\infty, t)]^{1/2}$ is plotted vs film thickness in Fig. 3 from which we extract a value of $\beta_{eff}=0.7\pm0.05$ for growth in the saturation rage (t=100-500 nm) on [100]-miscut substrates. For growth on singular substrates, $\beta_{eff}=0.6\pm0.05$ over the same film thickness range followed by a rapid increase in βeff to values>1 for t>500 nm. α_{eff} and β_{eff} values for [110]-miscut samples were found to be similar to those of the [100]-miscut sample with slightly larger $[G(\infty, t)]^{1/2}$ values as shown in Fig. 3. The exponents obtained from our measurements are all larger than those predicted by scaling theories for ballistic aggregation "hit and stick" (α=1/3, β=1/5).[17] They also do not agree with the hyperscaling

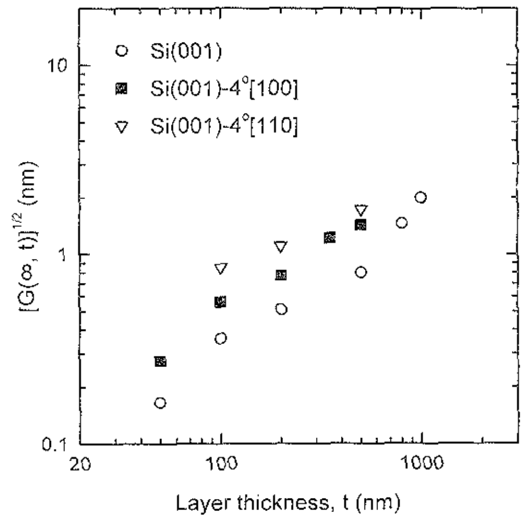

Fig. 3 Saturated root-mean correlated height-difference $[G(\infty, t)]^{1/2}$ vs film thickness for epitaxial Si films grown at T_s=300℃ on nominally-singular Si(001), Si(001)-4° [100], and Si(001)-4° [110] substrates.

relationship, $2\alpha=(\alpha/\beta-2)$,[18] derived for deposition under conditions in which deposited adatoms are allowed to relax by surface diffusion into positions of higher bonding coordination.

The instability giving rise to the development of the observed growth mounds separated by a well-defined length scale cannot be explained simply by statistical fluctuations in the growth flux.[1-3] This is easily demonstrated using the simple model[3] to estimate the magnitude of height fluctuations due to noise combined with surface smoothening by diffusion. Root-mean square surface roughness values obtained for a 500-nm-thick film grown on a [100]-miscut substrate, for example, are approximately a factor of 30 smaller than our measured values. Moreover, the use of vicinal substrates, in which the average terrace width is of the order of adatom mean free paths

(estimated to be 2-3 nm at 300℃), would be expected to lead toward stable step-flow growth rather than to the growth instabilities we observe.

We propose that the primary source of the growth instability during low-temperature deposition on singular and miscut Si(001) surfaces stems from the anisotropy in diffusion along and across dimer rows[19,20] combined with adatom trapping near descending A-step edges[21] *leading to enhanced "extrinsic" island* nucleation. In the case of the miscut substrates, where the step density is high, we expect that extrinsic island nucleation rates will far exceed *the rate of "intrinsic" random terrace* nucleation resulting in a larger roughness and a much earlier development of growth mounds. This tendency is consistent with both our AFM images and the results in Fig. 3 showing that the absolute values of the root-mean height-difference correlation functions were larger, at comparable film thicknesses, on the vicinal surfaces. Instabilities leading to the formation of mounds have also been reported during low-temperature MBE of Ge[3] in the two-dimensional (2D) multilayer growth mode on near-singular (001) substrates. However, the role of steps in influencing the evolution of surface roughening in this growth mode, where high terrace nucleation rates minimize substrate-tilt induced diffusion currents, has not been addressed.

The mound morphology observed during *2D multilayer growth* in this experiment is different from that observed during the elevated-temperature *layer-by-layer* molecular-beam epitaxial (MBE) growth of GaAs on near-singular GaAs(001) substrates. The presence of a "diffusion bias"[22] during growth in the step-flow mode is predicted to stabilize smooth growth surfaces due to a substrate-tilt-dependent diffusion current while terrace nucleation destabilizes the growth surface by reducing the current and leading to layer-by-layer growth with the production of mound or pyramid-like structures.[2] In this case, steps stabilized the growth surface.

3. 2 Surface morphology and roughness evolution during $Si_{0.7}Ge_{0.3}(001)$ growth

3. 2. 1 Evolution of surface morphology and roughness as a function of T_s

AFM was used to investigate the effects of film growth temperature, 200-550℃, on the surface morphology of 100-nm-thick $Si_{0.7}Ge_{0.3}$ layers grown on nominally singular Si(001) substrates. The previous XRD and TEM measurements[13] showed that alloys deposited at T_s 400℃ were fully strained, while the films grown at 440 and 475℃ were partially relaxed. The 550℃ layer was almost fully relaxed. The AFM image in Fig. 4(a) shows that the surface of the T_s=475℃ alloy exhibits strain-induced roughening in which relatively large rounded-shaped islands, with an average separation of ≃180 nm, develop in order to partially reduce the total strain energy in the system. Increasing T_s to 550℃ resulted in island coalescence with the average island separation increasing to ≃200 nm. In contrast, films grown in the very low-temperature regime, T_s < 325 ℃ exhibited kinetic surface roughening associated with 2D multilayer growth. A typical result is shown in Fig. 4(d) for T_s=200℃. The

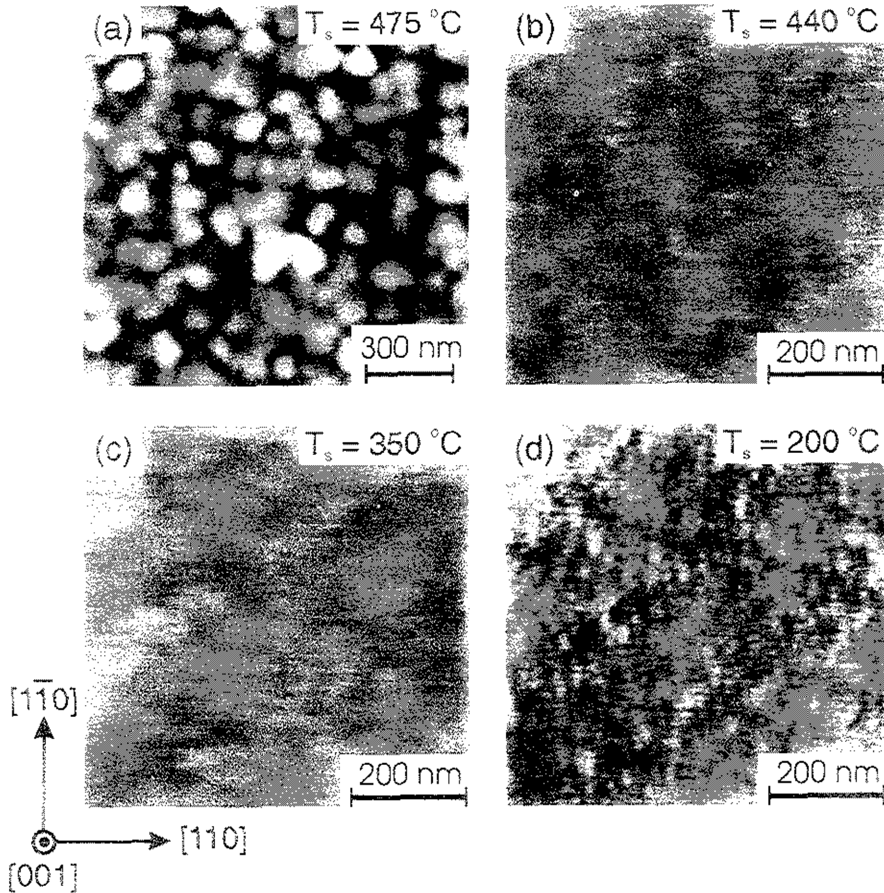

Fig. 4. AFM images of the surfaces of 100-nm-thick epitaxial $Si_{0.7}Ge_{0.3}$(001) layers on Si(001). Film growth temperatures T_s and black-to-white image scales are: (a) 475℃, 13 nm ; (b) 440℃, 5 nm ; (c) 350℃, 5 nm ; and (d) 200℃, 5 nm.

features are much smaller, with lateral separations of order 20 nm, and less well defined than those due to strain-induced 3D islanding. In fact, the surface morphology of the 200℃ $Si_{0.7}Ge_{0.3}$(001) layer is very similar to that observed for low-temperature homoepitaxial Si (001) grown at T_s=300℃ shown in Fig. 1(a).

In the intermediate growth temperature range, 325≤T_s≤450℃, film surfaces are smooth with no detectable features. Examples are shown in Figs. 4(b) and 4(c) for T_s=440 and 350℃.

Height difference correlation functions $G(\rho, t)$ were calculated from AFM images, including the ones shown in Fig. 4, of 100-nm-thick $Si_{0.7}Ge_{0.3}$ layers grown as a function of T_s. Using a least squares fit to analyze the data in a log-log plot of $[G(\rho\rightarrow\infty)]^{1/2}$ vs ρ (not shown here), α was found to be 0.75±0.02 at T_s=200-250℃, 0.60±0.02 at T_s=300-440℃, and 0.90±0.03 at T_s=475-550℃.

The saturated height-difference correlation

function $[G(\rho\to\infty)]^{1/2}$ is plotted as a function of film growth temperature T_s in Fig. 5. As expected based upon the AFM images, $[G(\rho\to\infty)]^{1/2}$ values are largest for films grown in the high-temperature regime with $[G(\rho\to\infty)]^{1/2}$ 2.3nm at T_s=475℃ and 1.2 nm at 550℃. Decreasing T_s into the kinetic roughening regime, 325℃, resulted in a dramatic decrease in $[G(\rho\to\infty)]^{1/2}$ values to ≃0.4 and 0.2 nm at T_s=200 and 250℃, respectively. However, the surface roughness decreased even further at intermediate deposition temperatures, T_s=350-435℃, to yield $[G(\rho\to\infty)]^{1/2}$ values less than 0.13 nm, indicative of growth proceeding in a layer-by-layer mode. Note that at T_s=300℃ $[G(\rho\to\infty)]^{1/2}$ is much lower for $Si_{0.7}Ge_{0.3}$ than for Si films grown by the same technique.

Decreasing the growth temperature allows surface kinetic processes to assume an increasingly important role in determining surface morphology. Adatom mean free paths become shorter leading to higher island nucleation rates on terraces, a smaller average island size, and smoother surfaces at all film thicknesses. However, at very low temperatures, 300℃ in this case, barriers to crossing step edges[20,21] begin to significantly inhibit interlayer mass transport thereby enhancing kinetic roughening associated with 2D multilayer growth. A comparison of the present low-temperature $Si_{0.7}Ge_{0.3}$ results with those of homoepitaxial Si(001) films in section 3.1 in the kinetic roughening regime shows that the alloy film surface is smoother than that of pure Si.

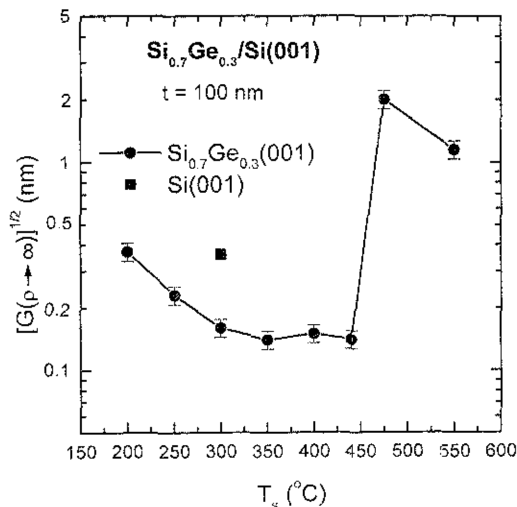

Fig. 5 Saturated root-mean correlated height-difference $[G(\infty, t)]^{1/2}$ vs the growth temperature T_s of 100-nm-thick epitaxial $Si_{0.7}Ge_{0.3}$(001) films on Si(001).

At growth temperatures between those corresponding to the kinetic and strain-induced roughening regimes, we have shown that there is a reasonably wide temperature window (the value of which will depend upon alloy concentration and film growth rate) where extremely-smooth fully-strained $Si_{1-x}Ge_x$ alloys can be grown on Si(001). $[G(\rho\to\infty)]^{1/2}$ values for 100-nm-thick $Si_{0.7}Ge_{0.3}$(001) layers grown at 350-435℃, for example, are only 0.13 nm which is comparable to that of the starting homoepitaxial Si(001) buffer layer, 0.09 nm. Even for alloy layers with thicknesses near h_c in this growth temperature range (e.g., t=650 nm at 350℃ and 180 nm at 435℃), $[G(\rho\to\infty)]^{1/2}$ is less than 0.45 nm. The use of kinetics to control surface roughening during epitaxy at intermediate growth temperatures offers not only the potential for decreasing the overall thermal budget during device fabrication.

3.2.2 Evolution of surface morphology and roughening as a function of film thickness

The evolution of surface roughening on $Si_{0.7}Ge_{0.3}$(001) was also investigated as a function

of film thickness t. In the high-temperature strain-induced roughening regime, the surface roughness increases rapidly. Fig. 6 shows typical AFM images of films grown at T_s=550 ℃. An islanded surface structure is already apparent at t=7.5 nm. However, as shown in Fig. 7, $[G(\infty, t)]^{1/2}$ increases at a rapid rate over this thickness range, from 0.1 nm for the starting Si(001) buffer-layer surface to 0.5 nm for the 7.5-nm-thick alloy layer to 2.3 nm at t=15 nm. Thus, the islands grow rapidly in the vertical direction with no indication in AFM images of significant coarsening.

A further increase in t to 30 nm has little additional effect on the surface roughness. However, as shown in Fig. 6(b), the coherently-strained islands are now well-developed with edges along ⟨100⟩ directions and some indication of facetting. Analyses of AFM micrographs indicate that the four 90o-rotated cusp surfaces contain segments oriented at or near {105} facet planes (see also Fig. 8(a)).

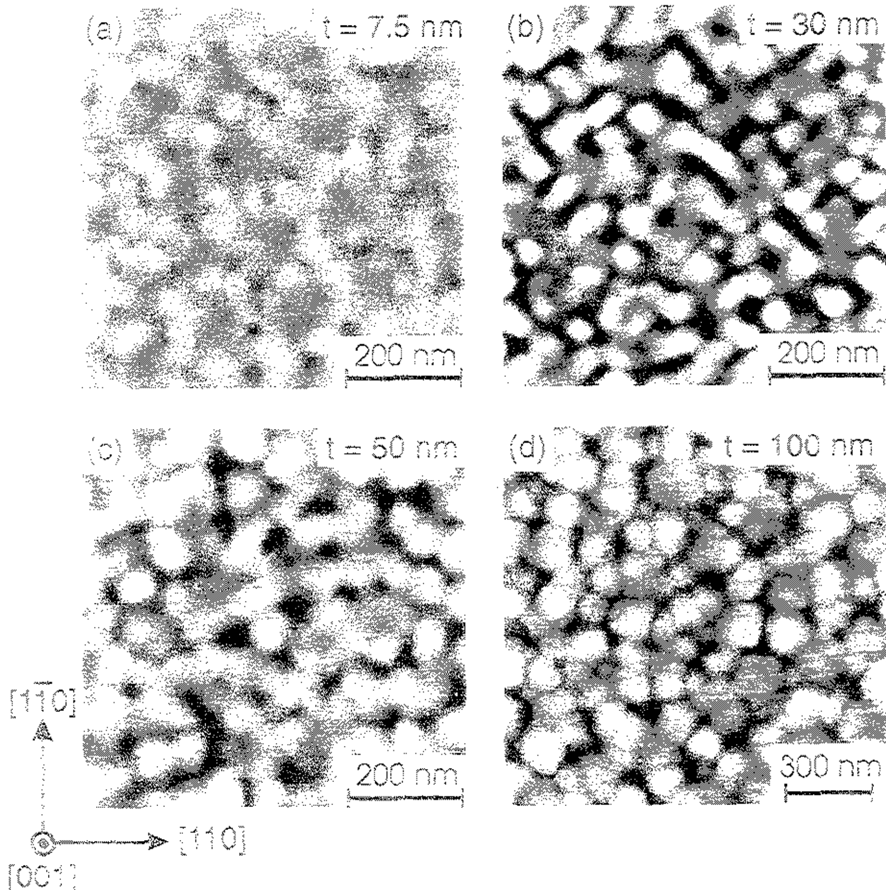

Fig. 6 AFM images of the surfaces of epitaxial $Si_{0.7}Ge_{0.3}$(001) grown on Si(001) at T_s=550℃. Film thicknesses t and black-to-white gray image scales are: (a) 7.5 nm, 4 nm ; (b) 30 nm, 8 nm ; (c) 50 nm, 3 nm ; and (d) 100 nm, 4 nm.

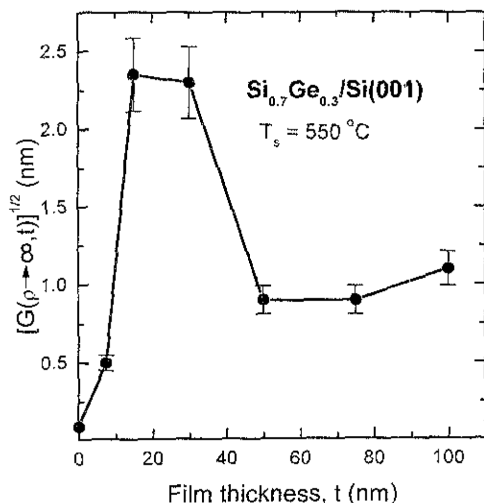

Fig. 7 Saturated root-mean height-difference correlation functions $[G(\infty, t)]^{1/2}$ vs the thickness t of epitaxial $Si_{0.7}Ge_{0.3}$(001) films grown on Si(001) at T_s=550℃.

As the $Si_{0.7}Ge_{0.3}$ film thickness t exceeded the critical value for the formation of interfacial misfit dislocations ($h_c\simeq35$ nm at T_s=550 ℃), Figs. 6(c) and 6(d) show that the surface of films grown on nominally-singular Si(001) substrates quickly smoothened through island coalescence. As shown in Fig. 7, $[G(\rho\rightarrow\infty)]^{1/2}$ decreased from≃2.3 nm for a strained layer with t=30 nm to 0.8 nm for a partially relaxed layer with t=50 nm while the average island separation increased from≃65 nm to 90 nm. In the absence of strain during growth in this high-temperature thermodynamically-controlled regime, smoothening occurs to minimize the total surface area. As expected, based upon the above discussion, the relaxation of film strain also reduces the tendency for islands to develop ⟨100⟩-oriented pyramidal shapes; instead they evolve toward more rounded shapes to further reduce the total surface area.

3.2.3 Effect of substrate vicinality

Strained 30-nm-thick $Si_{0.7}Ge_{0.3}$ films were grown at T_s=550℃ on nominally-singular Si (001) and vicinal Si(001) substrates miscut either 4° toward [100] or 4° toward [110]. Typical AFM images are shown in Fig. 8. The 3D islands in films grown on singular Si(001) substrates (Fig. 8(a)), as noted in the previous section, tend to be bounded by ⟨100⟩ edges and aligned in rows along 100 directions. Similar in-plane morphological characteristics were observed in films grown on Si(001)-4° [100] miscut substrates (see Fig. 8(b)) where the tendency of the islands to form along the elastically soft ⟨100⟩ directions is even stronger. However, Fig. 8(c) reveals that surface features in films grown on Si(001)-4°[110] miscut substrates are more rounded with a tendency to align along ⟨110⟩ rather than ⟨100⟩ directions.

Two-dimensional histograms of the directions of vector normals to the surfaces of the islands shown in the corresponding AFM micrographs are also plotted in Figs. 8(d), (e), and (f). Films grown on Si(001) have surface normals which are primarily within 7° around [001] but with components which range out to the ⟨105⟩ poles indicating a weak tendency for facetting (see Fig. 8(d)). The intensity distributions in the outer four lobes in Fig. 8(d) are centered near the ⟨105⟩ poles marked by "+" signs. XTEM micrographs of this sample obtained along [100] (not shown here) show that the surface normals near ⟨105⟩ poles result from cusps or trenches formed at intersections between islands. The XTEM micrograph (not shown here) and AFM histogram in Fig. 8(e) show that the cusp-like features[23] are deeper and the propensity toward facetting is greatly enhanced for films grown on 4°[100] substra

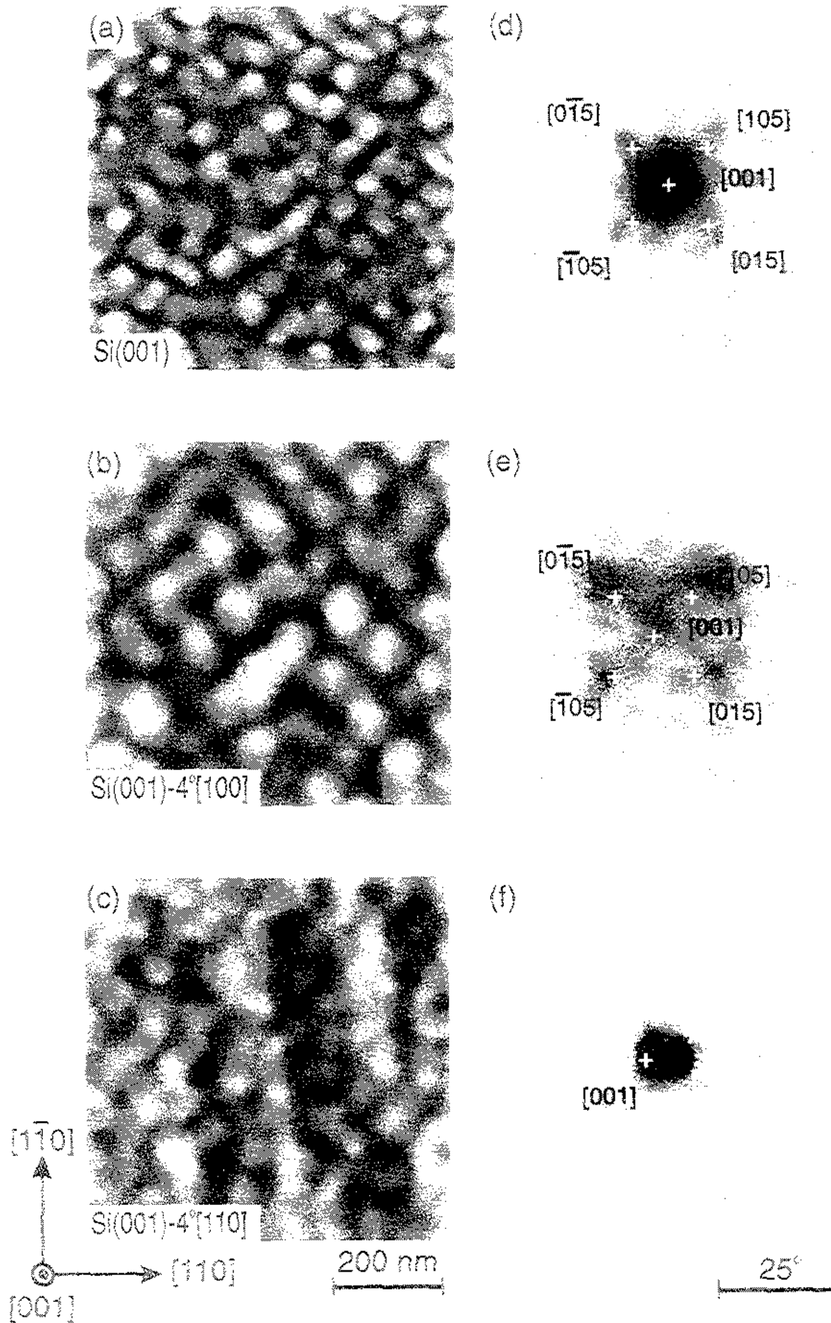

Fig. 8 AFM images of the surfaces of 30-nm-thick epitaxial $Si_{0.7}Ge_{0.3}$ layers grown on (a) Si(001), (b) Si(001)-4°[100], and (c) Si(001)-4°[110] substrates at T_s~550℃. Black-to-white image scales are: (a) 13 nm, (b) 35 nm, and (c) 10 nm. (d), (e), and (f) are histograms showing the directions of vector normals to the surfaces of the islands shown in (a), (b), (c), respectively.

tes. In contrast, Fig. 8(f) shows that for alloys grown on Si(001)-4 [110], essentially all surface normals are within ±6° of the center lobe with little indication of facetting.

The $[G(\rho\rightarrow\infty)]^{1/2}$ values obtained from $[G(\rho)]^{1/2}$ vs ρ plots (not shown here) indicate that the surface roughness of the (001)-4° [110] film, 1.7 nm, was similar to slightly smaller that of the (001) layer, 2 nm, but with a larger average island separation, $\langle d\rangle \simeq$ 95 nm vs ≃65 nm for (001). The roughness of the more strongly facetted (001)-4° [100] film was very much larger, ≃8 nm with $\langle d\rangle \simeq 110$ nm, than either of the other two.

{105} facetting has been observed previously during the growth of 20- to 175-nm-thick $Si_{1-x}Ge_x$ (x=0.15-0.35) layers on Si(001) by chemical vapor epitaxy (CVD) at T_s=500-750 ℃[8-10] and the MBE growth of Ge on Si(001) at T_s= 200℃.[4,24] A STM study of the MBE Ge layers showed that islands on (001)-2.5°[100] Si have edges more closely oriented along ⟨100⟩ directions than those on Si(001), similar to our observations for $Si_{0.7}Ge_{0.3}$. STM images[4,24] revealed that the Ge {105} facets consist of narrow (001) terraces separated by single-atom-height steps along ⟨100⟩ directions. The terraces, with width 5/4 of the Si lattice parameter, contain two Si dimers oriented such that the dimer bonds are 45° to the step edges. Based upon this observation, Knall et al.[24] suggested that {105} facet formation allows the compressive stress in a given terrace to be partly compensated elastically by the 90°-rotated dimer pair in the next terrace down. Effective stress relief may explain the kinetic pathway to leading to formation of {105} facetting rather than lowet energy facet surfaces such as, for example, the {113} which has been observed during the homoepitaxial growth of Ge(001).[25,26]

4. CONCLUSIONS

Low-temperature Si epitaxy is unstable on both singular and vicinal surfaces and leads to the development of well-defined growth mounds. The growth surfaces are not self-affine and the evolution of surface roughness is inconsistent with conventional scaling laws for kinetic roughening. The most important finding of this research, however, is that contrary to results obtained for high temperature epitaxy in the step flow regime, the Si(001) growth surface is more unstable on vicinal than on singular substrate surfaces during growth in the 2D multilayer mode.

Strain-induced roughening was found to be dominant at high growth temperatures ($T_s\geq$ 450℃) with surface roughness increasing as a function of film thickness t and then decreasing again due to island coalescence as t approaches the critical layer thickness for strain relaxation. Growth on [100]-miscut substrates enhanced the formation of ⟨100⟩ -bounded 3D islands with {105} facetting, while the use of [110]-miscut substrates suppressed the tendency for facetting. At low growth temperatures ($T_s\leq$250℃), the surface roughens kinetically but at much lower rates than observed for high-temperature strain-induced roughening. In the intermediate temperature range, the growth surface remains relatively smooth even near the critical layer thickness for strain relaxation.

References

1. J. Lapujoulade, Surf. Sci. Repts. 20, 191 (1994) ; J. Krug and H. Spohn, in *Solids Far From the Equilibrium*, edited by C.

Godr he (Cambridge Univeristy Press, Cambridge, England, 1991), pp. 479 ; T. Vicsek, Fractal Growth Phenomena (World Scientific, Singapore, 1991), pp. 386.

2. M. D. Johnson, C. Orme, A. W. Hunt, D. Graff, J. Sudijino, L. M. Sander, and B. G. Orr, Phys. Rev. Lett. 72, 116 (1994).
3. J. E. Van Nostrand, S. J. Chey, M.-A. Hasan, D. G. Cahill, and J. E. Greene, Phys. Rev. Lett. 74, 1127 (1995).
4. Y.-W. Mo, D. E. Savage, B. S. Swartzentruber, and M. G. Lagally, Phys. Rev. Lett. 65, 1020 (1990).
5. K. Sakamoto, T. Sakamoto, S. Nagao, G. Hashiguchi, K. Kuniyoshi, and Y. Bando, Japn. J. Appl. Phys. 26, 666 (1987).
6. C. W. Snyder, J. F. Mansfield, and B. G. Orr, Phys. Rev. B 46, 9551 (1992).
7. K. Sakamoto, T. Sakamoto, S. Nagao, G. Hashiguchi, K. Kuniyoshi, and Y. Bando, Japn. J. Appl. Phys. 26, 666 (1987).
8. A. J. Pidduck, D. J. Robbins, A. G. Cullis, W. Y. Leong, and A. M. Pitt, Thin Soid Films 222, 78 (1992).
9. A. G. Cullis, D. J. Robbins, A. J. Pidduck, and P. W. Smith, J. Cryst. Growth 123, 333 (1992).
10. M. A. Lutz, R. M. Feenstra, P. M. Mooney, and J. O. Chu, Surf. Sci. 316, L1075 (1994).
11. D. E. Jesson, K. M. Chen, S. J. Pennycook, T. Thundat, and R. J. Warmack, Science 268, 1161 (1995).
12. N.-E. Lee, G. Xue, and G. E. Greene, J. Appl. Phys. 80, 769 (1996).
13. N.-E. Lee, M. Matsuoka, M. R. Sardela, Jr., F. Tian, and G. E. Greene, J. Appl. Phys. 80, 769 (1996).
14. N.-E. Lee, G. A. Tomasch, and J. E. Greene, Appl. Phys. Lett. 65, 3236 (1994).
15. The effects of using a finite tip radius can be estimated based upon a model developed by J. E. Griffith and D. A. Grigg, J. Appl. Phys. 74, R83 (1993). Assuming the worst case in our experiments with a 40 nm tip radius results in $[G(\rho, t)]^{1/2}$ being underestimated by 20% for films with mound separations d < 20 nm and 10% for films with larger mound separations. These uncertainties, which are inherent in the AFM measurements, were included in determining the overall uncertainties quoted in the text for the effective roughening and growth exponents α_{eff} and β_{eff}.
16. H-N. Yang, G.-C. Wang, and T.-M. Lu, Diffraction From Rough Surfaces and Dynamic Growth Fronts (World Scientific Publishing Co., Singapore, 1993), pp. 136.
17. F. Family, Physica A 168, 561 (1990).
18. D. E. Wolf and J. Villain, Europhys. Lett. 13, 389 (1990) ; M. Schroeder, M. Siegert, D. E. Wolf, J. D. Shore, and M. Plischke, ibid. 24, 563 (1993).
19. Y.-W. Mo and M. G. Lagally, Surf. Sci. 248, 313 (1991) ; Y.-W. Mo, J. Kleiner, M. B. Webb, and M. G. Lagally, ibid. 268, 275 (1992).
20. C. Roland and G. H. Gilmer, Phys. Rev. B 46, 13437 (1992) ; Phys. Rev. Lett. 67, 3188 (1991).
21. Z. Zhang, Y.-T. Lu, and H. Metiu, Phys. Rev. B 46, 1917 (1992).
22. J. Villain, J. Phys. I, 1, 19 (1991).
23. D. E. Jesson, S. J. Pennycook, J.-M. Baribeau, and D. C. Houghton, Phys. Rev. Lett. 71, 1744 (1993).
24. J. Knall and J. B. Pethica, Surf. Sci. 265, 156 (1992).
25. T. R. Bramblett, Q. Lu, N.-E. Lee, N. Taylor, M.-A. Hasan, and J. E. Greene, J. Appl.Phys. 77, 1504 (1995).
26. C. Tatsuyama, T. Terasaki, H. Obata, T. Tanbo, and H. Ueba, J. Cryst. Growth 115, 112 (1991).